

## Preequilibrium particle emission and the giant-dipole resonance in Sn nuclei

M. P. Kelly, J. F. Liang, A. A. Sonzogni, K. A. Snover, J. P. S. van Schagen, and J. P. Lestone  
*Nuclear Physics Laboratory, University of Washington, Seattle, Washington 98195*  
(Received 16 June 1997)

Light charged particles from  $^{18}\text{O}+^{100}\text{Mo}$  reactions at 200 MeV bombarding energy have been measured in singles and in coincidence with high-energy  $\gamma$  rays ( $\geq 10$  MeV) produced primarily in the decay of the giant-dipole resonance. Particle spectra are analyzed in terms of a moving source fit to decompose preequilibrium and evaporative components. Preequilibrium particle multiplicities and energies indicate a reduction in the compound nucleus excitation energy of approximately 20% and a loss of mass of approximately three mass units relative to complete fusion. The energy lost to preequilibrium emission is shown to affect significantly the strength, width, and centroid energy of the giant-dipole resonance deduced from fits to high-energy  $\gamma$ -ray emission spectra. Evaporation residue cross sections were measured for the same reaction from 100 to 217 MeV in order to determine the fusionlike event cross section. [S0556-2813(97)03911-3]

PACS number(s): 25.70.Jj, 25.70.Gh, 24.30.Cz

### I. INTRODUCTION

The proper characterization of hot nuclei formed in heavy-ion collisions is essential to an understanding of the giant-dipole resonance (GDR) at high excitation energy. Measurements in the past ten years indicate a saturation of the GDR  $\gamma$ -ray yield above an excitation energy of approximately 250 MeV in mass  $A \sim 110$  nuclei and have been used as evidence of a limiting temperature for collective motion in hot nuclei [1–3]. There remains much uncertainty in the behavior of the GDR width with increasing excitation energy. Experimental studies of Sn nuclei and nearby masses, however, show evidence for a saturation of the width at a temperature of approximately  $T \sim 3$  MeV [4–6]. Theoretically, the contributions to the width from thermal shape fluctuations and spin-induced deformations are expected to saturate [7,8]. The role of the spreading width of the GDR, which may increase with excitation energy, is less well understood [9,10]. In addition, there is a contribution to the width of the GDR strength function of (twice) the particle evaporation width [11].

Any experimental investigation of the GDR relies on knowledge of the properties of the initial compound nucleus; in particular, the excitation energy, mass, and charge. In addition, if one plans to deduce the GDR strength from the absolute cross section for high-energy  $\gamma$ -ray production, then the fusion cross section must be known. One technique used to estimate the initial excitation energy involves measurement of the velocities of fusionlike residues and, through the use of a model, a calculation of the excitation energy. However, the separation of single nucleon preequilibrium events is difficult due to straggling in the target and the unavoidable smearing of the residue spectrum from particle evaporation. Another method uses the temperature deduced from backward angle particle spectra. This second method depends on knowledge of the exact value of the nuclear level density parameter in addition to an accurate extraction of the evaporative particle component. The large systematics that exists for linear momentum transfer in heavy-ion collisions [12,13] have also been used to estimate the amount of incomplete

fusion. This technique will tend to underestimate the effect of the energy loss due to incomplete fusion as it is largely insensitive to single nucleon preequilibrium emission.

This work presents the direct measurement of light charged particles both in singles and in coincidence with high-energy  $\gamma$  rays from GDR decay, where the  $\gamma$  rays are used as a tag for fusionlike-evaporation events. The coincidence measurement addresses the question of what fraction of the preequilibrium particles are associated with fusionlike (complete+incomplete fusion) events. Previous measurements have used discrete  $\gamma$ -ray lines characteristic of the decay of individual residual nuclei to associate preequilibrium particles with specific decay channels [14,15]. Such measurements show a decrease in the evaporative particle multiplicity due to preequilibrium emission. Inclusive particle measurements over a wide range of bombarding energies and target-projectile combinations indicate an insensitivity of preequilibrium emission to the details of the projectile and the target [16] and a scaling of the preequilibrium particle multiplicity with the bombarding energy above the Coulomb barrier [17]. A small contribution to preequilibrium emission from fragments heavier than the  $\alpha$  particle has been identified [18]. This is unlikely to be important in the current analysis as the cross sections are expected to be small compared to those of light particles, and in addition, the energy carried away by heavy preequilibrium fragments is large and thus greatly reduces the likelihood of high-energy GDR  $\gamma$ -ray emission.

The goal of this investigation was to measure experimentally the preequilibrium charged particles associated with fusionlike events and, in a separate measurement of evaporation residues, to determine the evaporation residue excitation function for  $^{18}\text{O}+^{100}\text{Mo}$ . A detailed analysis of the effect of preequilibrium emission on GDR parameters deduced from  $\gamma$ -ray emission spectra is presented. The reaction  $^{18}\text{O}+^{100}\text{Mo} \rightarrow ^{118}\text{Sn}$  (in the case of complete fusion) was chosen for study as compound nuclei in the Sn mass region have been and continue to be the subject of GDR studies [2–4,19]. GDR emission in this reaction is also the subject of a current study [20].

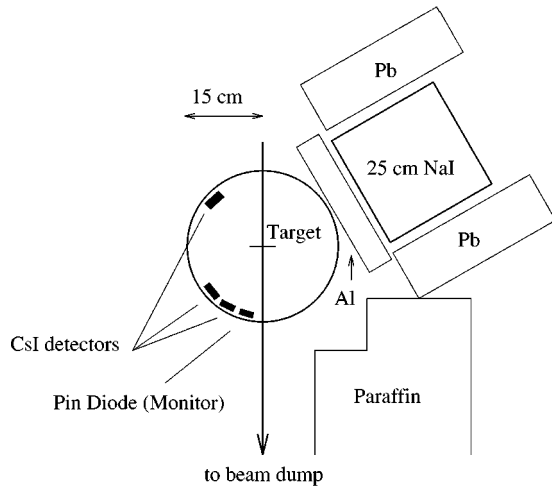


FIG. 1. Schematic of experimental apparatus for the coincidence measurements.

## II. EXPERIMENT

The measurements were performed at the University of Washington Nuclear Physics Laboratory using the FN Tandem Van de Graaff as injector for the Superconducting Linear Accelerator. For particle- $\gamma$ -ray coincidence measurements, a 200 MeV  $^{18}\text{O}$  beam was incident on a 5 mg/cm<sup>2</sup> self-supporting target enriched to 97.27% in  $^{100}\text{Mo}$ . Singles particle spectra were measured at 169 and 200 MeV bombarding energy for the same system.

The geometry of the experimental apparatus is shown in Fig. 1. Angular distributions of light charged particles at laboratory angles of 20°, 30°, 40°, 50°, 90°, and 140° were measured using three 1 cm thick CsI crystals coupled to PIN diode detectors. The size of the CsI detectors has been exaggerated in Fig. 1 for clarity. The actual acceptances of the three detectors were measured to be  $1.36 \times 10^{-2}$ ,  $1.36 \times 10^{-2}$ , and  $2.72 \times 10^{-2}$  sr going from forward to backward angles. Data were collected with the CsI detectors at 20°, 40°, and 140° and, in a second set of measurements, at 30°, 50°, and 90°. Light charged particles were identified using a pulse shape discrimination technique [21]. A typical spectrum of pulse shape versus energy is shown in Fig. 2. The energy calibration was performed using elastically scattered proton and  $\alpha$ -particle beams from a thin Au target.

$\gamma$  rays were detected in a 25 cm  $\times$  25 cm cylindrical NaI crystal placed at an angle of 110° relative to the beam axis and a distance of 23 cm from the target. The total solid angle  $\times$  efficiency product for detection of a high-energy  $\gamma$  ray was approximately 5% of  $4\pi$ . The crystal was shielded on the sides by a minimum of 10 cm of lead and from the beam dump by an additional 75 cm of paraffin. An aluminum shield approximately 5 cm thick was placed between the target and the NaI crystal to reduce the count rate for low-energy  $\gamma$  rays. Target-out measurements showed that the background from the beam dump, collimator, and target frame scattering was negligible. High-energy  $\gamma$  rays were separated from fast neutrons using a pulsed beam and the measured time-of-flight. The LINAC RF was used as a time reference. NaI energy spectra were calibrated using the 1.17 and 1.33 MeV  $\gamma$  rays from  $^{60}\text{Co}$  and the 4.44 MeV  $\gamma$  ray from a composite  $^{241}\text{Am}$ - $^9\text{Be}$  source. This procedure was

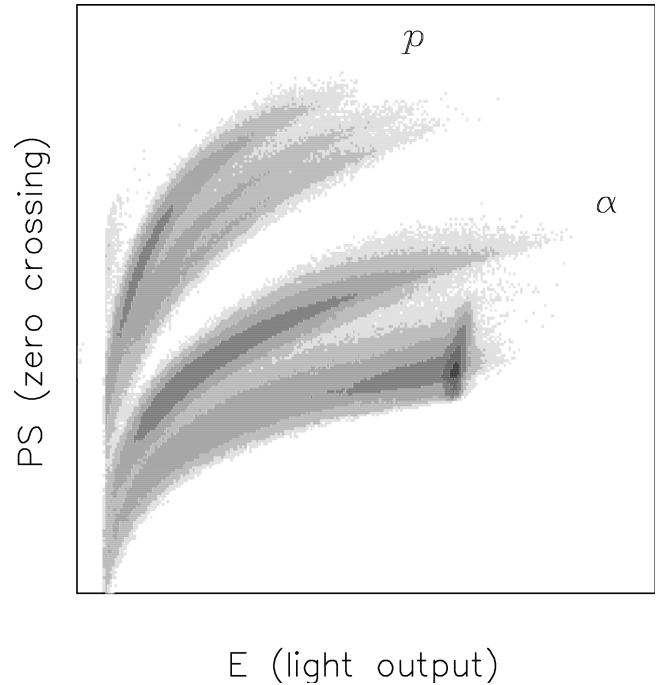


FIG. 2. Typical singles CsI pulse shape versus energy at  $\theta_{\text{lab}} = 20^\circ$ .

sufficient for present purposes since a precise calibration at higher energies was not needed.

To minimize the likelihood of accidental particle- $\gamma$ -ray coincidences a time-of-flight spectrum for particles relative to  $\gamma$  rays was measured and the requirement that particles and  $\gamma$  rays be coincident within a 150 ns window was made. An accidental coincidence spectrum corresponding to a coincidence between a  $\gamma$  ray and a particle from a following beam burst was accumulated, and a background due to accidental coincidences of approximately 3% of the total yield was subtracted from the particle spectra. The nearly complete suppression of elastically scattered beam in the 20° CsI coincidence spectra as compared to the singles spectra verified that the accidental coincidence rate was small.

In a separate measurement, an  $E$ - $\Delta E$  telescope consisting of silicon surface barrier detectors, was used to measure the angular distribution of evaporation residues from  $\theta_{\text{lab}} = 4^\circ$  to  $37^\circ$ . Residues resulting from collisions at bombarding energies from 100 to 217 MeV were measured. Evaporation residues were identified using energy and time-of-flight information and the data were normalized to the Rutherford scattering cross section measured by monitor detectors at  $\pm 7^\circ$  to the beam direction.

## III. DATA ANALYSIS

### A. Coincidence measurements

Coincidences between  $\gamma$  rays and light charged particles were recorded event by event and later analyzed to consider only those events where the  $\gamma$ -ray energy was 10 MeV or greater. This effectively filters out the nonfusion events, which produce few high-energy  $\gamma$  rays.

An unwanted effect when requiring detection of a high-energy  $\gamma$  ray in coincidence with a particle is a bias towards detection of low-energy particles relative to high-energy par-

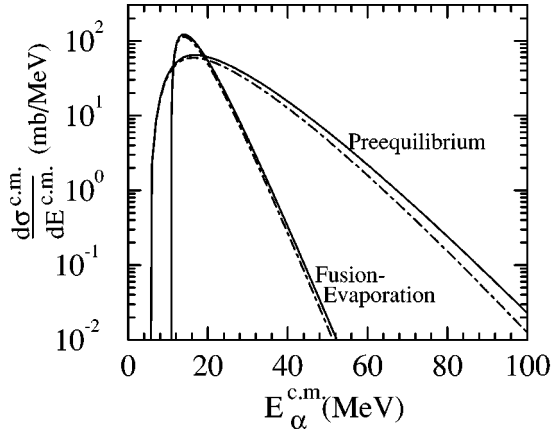


FIG. 3. Solid lines: angle integrated singles  $\alpha$ -particle spectra extracted from moving source fits for  $^{18}\text{O}+^{100}\text{Mo}$  at 200 MeV bombarding energy. Dot-dashed lines: expected spectral shape for  $\alpha$  particles in coincidence with high-energy  $\gamma$  rays (see text).

ticles. The origin of this bias may be understood as follows. When a preequilibrium particle is emitted, energy is lost to the compound system, leaving less energy for production of high-energy GDR  $\gamma$  rays. Clearly, the higher the energy of the emitted particle, the smaller the likelihood for subsequent emission of a high-energy  $\gamma$  ray. This leads to a differential suppression of high-energy particles relative to low-energy particles in the coincidence measurement. A quantitative estimate of the effect was made using the statistical model code CASCADE. First, a  $\gamma$ -ray spectrum for  $^{18}\text{O}+^{100}\text{Mo}$  at 200 MeV bombarding energy was calculated at the full fusion excitation energy of 174 MeV. Next,  $\gamma$ -ray spectra were calculated at successively lower compound nucleus excitation energies and mass, reduced by either one  $\alpha$  particle or one proton, reflecting the energy and mass loss due to preequilibrium emission. The calculated ratio of the high-energy  $\gamma$  ray yield at the reduced excitation energy to the yield at the complete fusion excitation energy is the factor by which the preequilibrium particle yield is suppressed in the coincidence measurements. In these estimates we assumed preequilibrium particles of a given energy carried away the same angular momentum as evaporated particles of the same energy. The results of this calculation applied to the  $\alpha$ -particle spectra contained in Fig. 3 are shown in the same figure. It can be seen from Fig. 3 that the reduction is less than 15% below 40 MeV particle energy and becomes large only at very high particle energies where the total charged particle cross section is small. Particle multiplicities extracted using coincidence data have been corrected for this effect, while data shown in Figs. 4, 5, 6, and 7 are raw data and have not been corrected.

### B. Moving source analysis

Though statistical model calculations may be used to predict evaporated particle cross sections, there exists no accurate model for the calculation of fast particle emission in the region of 10 MeV/nucleon bombarding energy. Fermi jet model calculations [22] have been used with success at higher energies for single nucleon preequilibrium emission [23], but overpredict the yield at lower energies [24]. Even in statistical model codes, uncertainty in particle transmission

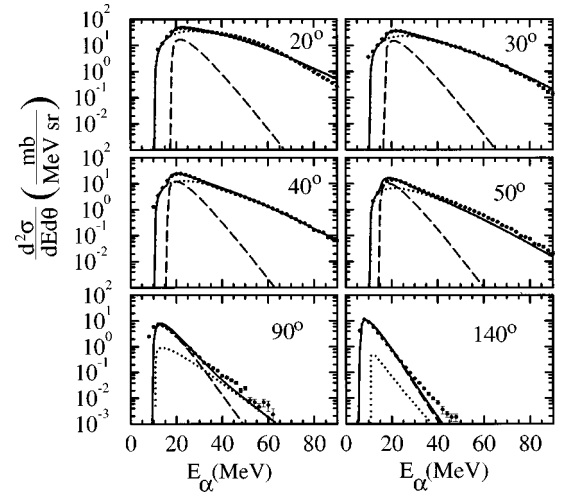


FIG. 4. Points: measured inclusive  $\alpha$ -particle spectra (laboratory frame) for  $^{18}\text{O}+^{100}\text{Mo}$  at 200 MeV bombarding energy. Dashed line: fit to the evaporative component. Dotted line: fit to the preequilibrium component. Solid line: the sum.

coefficients and level densities can lead to uncertainties of up to 50% in the absolute yield of evaporated particles. In this work we employ a phenomenological technique commonly used in the analysis of particle data; namely, the decomposition of particle spectra into fast and evaporative components based on a moving source fit [15,24]. Two ‘‘thermal’’ sources, one fixed at the compound nucleus velocity, the other with an adjustable velocity intermediate between the compound nucleus and the projectile velocity, are assumed. For the compound nucleus source we allow for a nonzero  $a_2$  coefficient [15] while the fast source is assumed to be isotropic in its rest frame. This parametrization is justified by the observation that particle spectra produced in calculations based on relatively detailed physical models, such as those in CASCADE and the Fermi jet model, can be reasonably parametrized in terms of a thermal source. The energy distribution of evaporated particles in the rest frame of the source is assumed to be Maxwellian and is given by

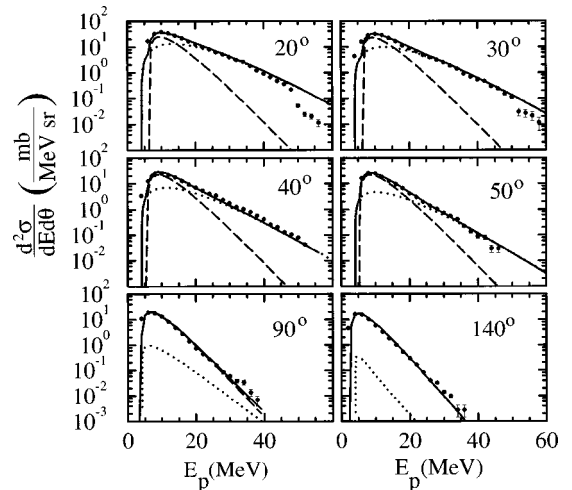


FIG. 5. Same as in Fig. 4 but for protons. At  $20^\circ$  and  $30^\circ$  the highest energy protons were not stopped in the CsI detectors. This region was not included in the fits.

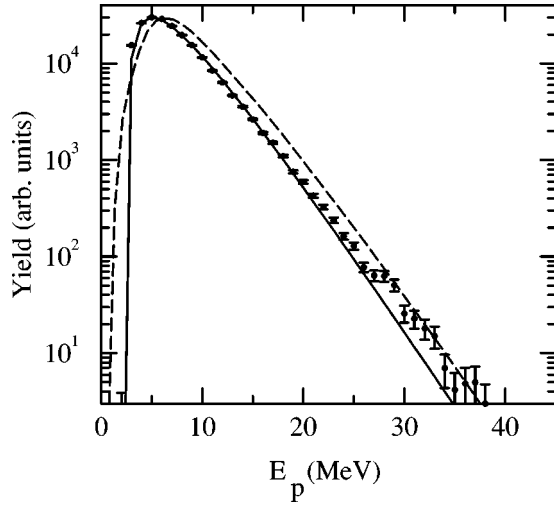


FIG. 6. Spectrum of protons emitted at  $\theta_{\text{lab}}=140^\circ$  for  $^{18}\text{O}+^{100}\text{Mo}$  at 200 MeV. Solid line: evaporative source spectrum from the moving source fit. Dashed line: CASCADE spectrum transformed to  $\theta_{\text{lab}}=140^\circ$ . The CASCADE yield has been renormalized to match the peak of the data.

$$\frac{d^2N}{d\Omega dE} = \frac{N}{4\pi T^2} (E - V_c) \times \exp[-(E - V_c)/T][1 + a_2 P_2(\cos\theta)], \quad (1)$$

where  $E$  is the particle energy,  $T$  is the apparent source temperature,  $V_c$  is associated with the height of the Coulomb barrier for particle emission, and  $\theta$  is the center-of-mass emission angle. The  $a_2$  coefficient was fixed using the relative yields at  $90^\circ$  and  $140^\circ$ , where the evaporative component is most accurately extracted. Integration over energy and solid angle gives  $N$ , the total number of evaporated particles. The distribution of fast particles is taken to be that for volume emission from a thermal source. Before consideration of the Coulomb barrier, the distribution of preequilibrium particles is written

$$\frac{d^2N_{\text{preeq}}}{d\Omega dE} = \frac{N_{\text{preeq}}}{2(\pi T_{\text{preeq}})^{3/2}} E^{1/2} \exp[-E/T_{\text{preeq}}] \quad (2)$$

in the emitting frame. This source is then transformed to the laboratory frame where the substitution  $E_{\text{lab}} \rightarrow E_{\text{lab}} - V_c$  is made. It should be emphasized that taking into account the Coulomb energy after transforming to the laboratory frame assumes that, at the time of preequilibrium particle emission, the Coulomb field is at rest in the laboratory frame. An equivalent statement is that, relative to the laboratory frame,

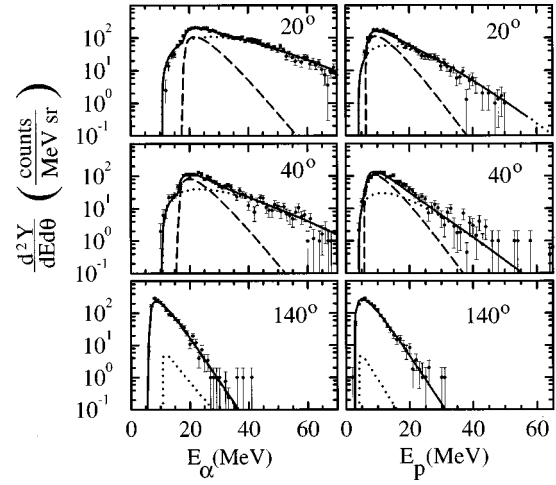


FIG. 7. Particle spectra (laboratory frame) in coincidence with a  $\gamma$  ray of energy 10 MeV or greater for  $^{18}\text{O}+^{100}\text{Mo}$  at 200 MeV bombarding energy. Left three panels:  $\alpha$  spectra. Right three panels: proton spectra. The dashed, dotted, and solid lines are the evaporative, preequilibrium, and summed components, respectively, extracted from a moving source fit.

the rest frame of the Coulomb field moves much more slowly than the rest frame of the preequilibrium source. It is, in fact, plausible that the Coulomb field, because it is generated by all charges in the colliding system, moves more slowly than the preequilibrium source (velocity  $\sim \frac{1}{2}v_{\text{beam}}$ ), which presumably involves only a small subset of all the target and projectile nucleons. In any case, this parametrization gives the best fit results to particle data in the region of the Coulomb energy. In fact, the parametrization allows us to fit the observed preequilibrium particles at forward angles at both low and high energies. Taking the Coulomb energy for each source to be in the source rest frame permits reasonable fits to particle spectra at high energy but is unsatisfactory in the region of the Coulomb barrier.

The expressions for each source were transformed to the laboratory using the relation

$$\frac{d^2N_{\text{lab}}}{d\Omega_{\text{lab}} dE_{\text{lab}}} = \left(\frac{E_{\text{lab}}}{E'}\right)^{1/2} \frac{d^2N'}{d\Omega' dE'}, \quad (3)$$

and fit to the measured particle data. It was found that the data could be fit with the same value of  $V_c$  for both sources. In addition, the evaporative source velocity was fixed to be that of the  $^{18}\text{O}+^{100}\text{Mo}$  center of mass. The remaining six parameters, listed in Table I, were treated as fit variables. Because a single particle spectrum measured at one angle did

TABLE I. Moving source fit parameters for the fits shown in Figs. 4 and 5. ‘‘Ratio’’ is the total yield of preequilibrium particles divided by the total yield of evaporated particles.  $V_c$  is the Coulomb energy parameter.  $v_1, v_2, T_1, T_2$  are the evaporative source velocity, preequilibrium source velocity, evaporative source temperature, and preequilibrium source temperature, respectively.  $v_{\text{c.m.}}$  is the center-of-mass velocity for complete fusion.  $a_2$  is an angular distribution coefficient [see Eq. (1)].

	Ratio	$V_c$ (MeV)	$v_1/v_{\text{c.m.}}$	$v_2/v_{\text{c.m.}}$	$T_1$ (MeV)	$T_2$ (MeV)	$a_2$
$\alpha$	$1.4 \pm 0.2$	10.8	1.0	3.5	3.2	6.1	$0.6 \pm 0.2$
proton	$0.3 \pm 0.1$	4.1	1.0	5.0	2.8	4.0	$0.0 \pm 0.1$

not always permit independent determination of all six parameters, the following procedure was used. First, spectra at  $\theta_{\text{lab}} = 140^\circ$  were fit with only the evaporative source to determine the Coulomb energy, multiplicity, and apparent source temperature for evaporative particle emission. The backward angle fits were found to be insensitive to the upper limit of energy in the fit, which is consistent with preequilibrium emission being a small contribution to the total yield at  $\theta_{\text{lab}} = 140^\circ$ . Second, parameters for the evaporative source were fixed and forward angle data were fit by varying the multiplicity, apparent temperature, and velocity of the preequilibrium source. The result is a fit based on six parameters that simultaneously describes the measured particle spectra at all angles. It should be pointed out that this prescription is phenomenological and the fit parameters may be only loosely associated with real physical quantities.

### C. Particle cross sections

The close proximity of the monitor to the target as shown in Fig. 1 meant that small shifts in the beam position on target or small shifts in the angle of the beam incident on target could lead to considerable error in the angle of the monitor to the beam direction. From considerations of detector and collimator geometry, it is estimated that the true monitor angle relative to the beam could differ by nearly  $\pm 1^\circ$  from the nominal value of  $10^\circ$ , which would introduce a large error when normalizing to the differential Rutherford scattering yield observed in the monitor. Thus, in a separate measurement, it was decided to measure the particle cross section accurately at one angle with a much improved detector geometry and use this measurement for normalization purposes. In this measurement monitors were placed at  $\pm 7^\circ$  relative to the beam axis and the distance from the target to the monitors was increased from 10 to 60 cm. The result was that systematic errors due to error in the monitor angle were reduced to the 1% level. With this improved geometry, the differential  $\alpha$ -particle cross section was measured at  $\theta_{\text{lab}} = 140^\circ$  using a single strip of area  $3.5 \text{ cm}^2$  of a segmented silicon surface barrier detector at a distance of 34 cm. Energy versus time-of-flight information was used for particle identification. The evaporated particle differential cross section from this measurement combined with the spectral shapes from  $\theta_{\text{lab}} = 20^\circ$  to  $\theta_{\text{lab}} = 140^\circ$  in the CsI measurements were used to obtain the particle cross sections.

## IV. RESULTS AND DISCUSSION

Inclusive  $\alpha$ -particle and proton spectra produced in the reactions of  $^{18}\text{O}$  incident on  $^{100}\text{Mo}$  at 200 MeV bombarding energy are shown in Figs. 4 and 5. The large excess of high-energy particles at forward angles is due to preequilibrium particle emission, while backward angle data are consistent with emission mostly from a single source, namely, the equilibrated compound nucleus. The moving source fit parameters for these data are given in Table I. To verify that the decomposition was reasonable, the extracted component for evaporated protons and  $\alpha$  particles was compared with the spectral shapes predicted by the statistical model code CASCADE run at the full fusion excitation energy and using Reisdorf's formulation of the level density parameter [25]. The spectral shapes were found to be very similar with the

main differences being a slightly hotter temperature and an elevated Coulomb energy for the CASCADE calculated spectra as shown in Fig. 6 for protons at  $\theta_{\text{lab}} = 140^\circ$ . The slightly lower experimental Coulomb energy might be due to the large thermally induced shape fluctuations which are ignored in the CASCADE calculations and, to a lesser extent, by the charge lost to preequilibrium emission.

$\gamma$ -ray tagged particle spectra along with moving source fits are shown in Fig. 7. The parameter of most interest is the ratio of the integrated yield of preequilibrium particles to that of evaporated particles. For  $^{18}\text{O} + ^{100}\text{Mo}$  at 200 MeV bombarding energy the ratio was determined to be  $0.7 \pm 0.1$  for the  $\gamma$ -ray tagged  $\alpha$ -particle spectra and  $0.25 \pm 0.05$  for the tagged proton spectra. The corresponding ratios for the untagged singles spectra are  $1.4 \pm 0.2$  for  $\alpha$  particles and  $0.27 \pm 0.04$  for protons. Interestingly, the coincidence  $\alpha$  spectra show only half as many preequilibrium  $\alpha$  particles relative to evaporative particles as the singles spectra indicating that only approximately half of the preequilibrium  $\alpha$  yield is associated with fusionlike events. This contrasts with the results of Gershel *et al.* [26] at a lower energy of 7.8 MeV/nucleon for  $^{16}\text{O} + ^{124}\text{Sn}$  where 90% of the fast  $\alpha$  yield was associated with fusionlike events. For singles proton spectra, the ratio of preequilibrium to evaporated protons is 0.27, the same ratio found in the coincidence measurement within experimental uncertainty. To convert these ratios into charged particle multiplicities two additional quantities, the evaporated particle cross sections and the total cross section for fusionlike events, are needed. Here we define multiplicity to be the number of particles per fusionlike event, where by fusionlike event we mean all complete+incomplete fusion events leading to a compound nucleus with most of the available energy and mass. From the second measurement with the improved detector geometry, the differential  $\alpha$ -particle cross section was measured to be  $89 \pm 2 \text{ mb/sr}$  at  $\theta_{\text{lab}} = 140^\circ$  and taken to be completely evaporative. The angular distribution in the laboratory is given approximately by  $W_{\text{evap}}(\theta) = A_0 [1 + a_1 P_1(\cos \theta) + a_2 P_2(\cos \theta)]$  where  $a_2$  is the value given in Table I. The  $a_1$  coefficient comes from kinematics and was calculated to be 0.22 averaged over  $\alpha$ -particle energy. This angular distribution gives an angle integrated yield of  $1060 \pm 80 \text{ mb}$  for the evaporated  $\alpha$ -particle cross section. Similarly for protons, the total evaporated cross section is determined to be  $1850 \pm 150 \text{ mb}$ . Indicated errors are dominated by the uncertainty in the  $a_2$  coefficient (see Table I) used to obtain the integrated cross sections.

### A. Fusionlike event cross sections

The angular distribution of evaporation residues for  $^{18}\text{O} + ^{100}\text{Mo}$  at 200 MeV bombarding energy is shown in Fig. 8. Similar distributions were measured at 100, 150, 169, 185, and 217 MeV. The fusionlike cross section is parametrized as a sum of two Gaussians [27]. The narrow Gaussian results from nuclei that have decayed by only neutron and proton channels while the broader Gaussian accounts for nuclei with one or more  $\alpha$  particles in the decay chain. The measured fusion excitation function is shown in Fig. 9 along with the default evaporation residue excitation function used in the statistical model code CASCADE which assumes a rotating liquid drop fission barrier [28]. For comparison, the calcu-

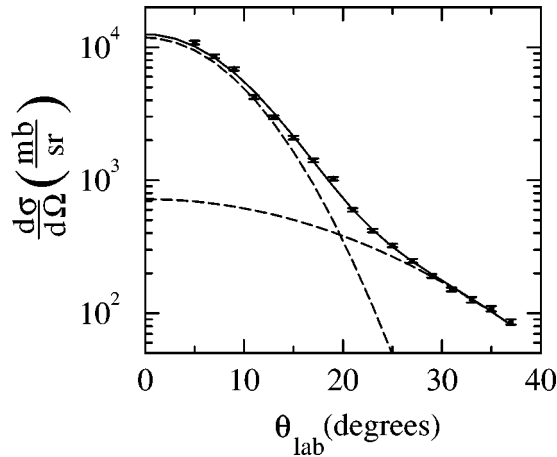


FIG. 8. Points: measured evaporation residue angular distribution for  $^{18}\text{O}+^{100}\text{Mo}$  at 200 MeV. The error bars are statistical. Solid curve: two Gaussian fit to the data. Dashed curves: individual Gaussian components.

lated residue excitation function using the Bass fusion model [29] together with the Sierk fission barrier [30] is also shown. The most striking feature of the measured excitation function is that the cross section continues to climb slowly up to the maximum measured bombarding energy of 217 MeV. If one naively considers the 1700 mb of residue cross section at 200 MeV bombarding energy to be complete fusion and assumes a sharp-cutoff model, one concludes that spin states up to  $82\hbar$  are populated, in conflict with liquid drop model calculations of the limiting angular momentum for fusion [28]. A more realistic interpretation is that collisions with very high relative orbital angular momentum lead primarily to incomplete fusion events where the fragment that does not fuse carries off some angular momentum. This is corroborated by earlier studies indicating that fast  $\alpha$ -particle emission, a large contributor to preequilibrium emission in these measurements, occurs in peripheral collisions [24,32–34].

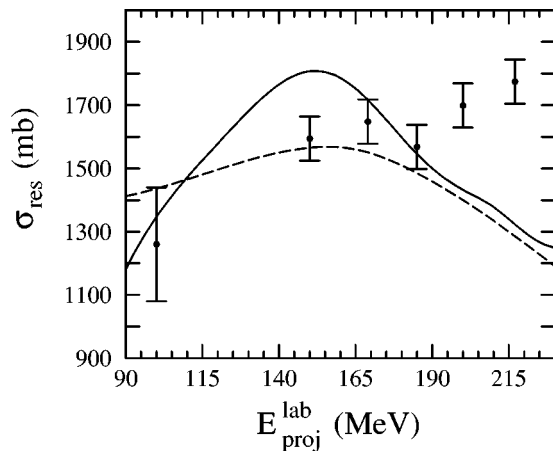


FIG. 9. Points: measured cross sections for fusionlike residues for from  $^{18}\text{O}+^{100}\text{Mo}$  as a function of bombarding energy. Error bars are calculated from the uncertainty in the Gaussian fit parameters (see Fig. 8). Solid line: the default fusion excitation function from CASCADE. Dashed line: Residue excitation function using Bass fusion together with the Sierk fission barrier.

TABLE II. Average kinetic energy  $E_k$ , binding energy  $E_{\text{bind}}$ , preequilibrium multiplicity  $M_{\text{fast}}$ , and average total energy lost  $E_{\text{lost}}$  to the compound system for each preequilibrium particle type. Multiplicities are those for  $\gamma$ -ray tagged data.  $E_k$  and  $E_{\text{bind}}$  are per preequilibrium particle.  $E_{\text{lost}}$  is the average energy lost to particles with the indicated multiplicity per fusionlike event.

	$E_k$ (MeV)	$E_{\text{bind}}$ (MeV)	$M_{\text{fast}}$	$E_{\text{lost}}$ (MeV)
$\alpha$	$24.5 \pm 0.5$	4.1	$0.45 \pm 0.07$	$12.9 \pm 2.0$
proton	$13.8 \pm 0.3$	10.0	$0.27 \pm 0.06$	$6.4 \pm 1.4$
neutron	$11.4^{\text{a}}$	9.3	$0.87 \pm 0.19^{\text{b}}$	$18.0 \pm 3.9$

<sup>a</sup>From a Fermi jet model calculation.

<sup>b</sup>The ratio of neutrons to protons from a Fermi jet model calculation multiplied by the measured proton multiplicity.

### B. Preequilibrium particle multiplicities

Evaporative particle multiplicities are found by dividing the evaporative particle cross sections by the residue cross section. The product of the evaporative particle multiplicity and the ratio of preequilibrium to evaporated particles for  $\gamma$ -ray tagged events gives the preequilibrium proton and  $\alpha$ -particle multiplicities. These values, along with the average preequilibrium proton and  $\alpha$ -particle kinetic energies and the average energy lost to the compound system per preequilibrium particle type are listed in Table II.

Preequilibrium neutron emission is known to exist in the bombarding energy region of 10 MeV/nucleon. Here we use the ratio of neutrons to protons from a Fermi jet model calculation together with our measured proton multiplicity to get a result for the neutron multiplicity reasonably consistent with previous experimental studies of light projectiles on heavy targets in the region of 10 MeV/nucleon bombarding energy.

Young *et al.* [15] determined the ratio of fast to evaporative neutrons to be 0.17 for  $^{16}\text{O}+^{154}\text{Sm}$  at 9.5 MeV/nucleon bombarding energy by performing a two source fit to measured neutron spectra. Using CASCADE to calculate the evaporated neutron multiplicity for this reaction, one deduces a fast neutron multiplicity of 1.3. In another measurement by Gavron *et al.* of  $^{13}\text{C}+^{157}\text{Gd}$  at 10.8 and 12.3 MeV/nucleon bombarding energies [35], the prompt neutron multiplicity was found, using a moving source analysis, to be 1.1 and 1.5, respectively. If one takes the ratio of preequilibrium neutrons to preequilibrium protons from a Fermi jet model calculation for  $^{18}\text{O}+^{100}\text{Mo}$  at 200 MeV bombarding energy, which is 3.22, together with our earlier result of  $0.27 \pm 0.06$  fast protons per fusionlike event, one gets  $0.87 \pm 0.19$  fast neutrons per fusionlike collision. For calculation of the energy lost to fast neutron emission we use the value of 0.87 for the multiplicity with an average kinetic energy of 11.4 MeV, as predicted by the Fermi jet model calculation.

The mean energy lost to the compound system per preequilibrium particle type is obtained by summing the average particle kinetic energy with its separation energy from  $^{118}\text{Sn}$  and taking the product of this quantity and the particle multiplicity. The total average energy lost to the compound system per fusionlike event is obtained by summing over the particle types (neutron, proton, and  $\alpha$ ). For the compound system formed in  $^{18}\text{O}+^{100}\text{Mo}$  at 200 MeV bombarding en-

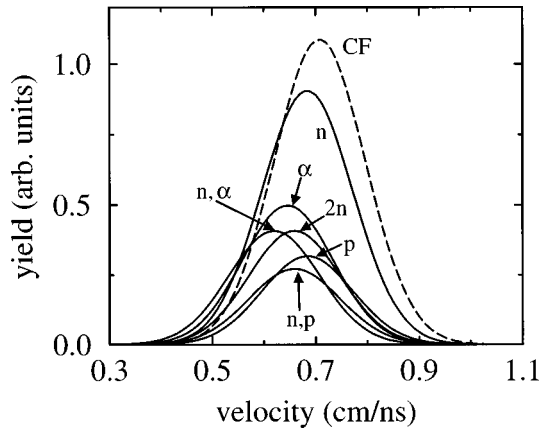


FIG. 10. Dashed line: evaporation residue velocity distribution from a PACE calculation for  $^{18}\text{O}+^{100}\text{Mo}$  at 200 MeV assuming complete fusion. Solid lines: residue velocity distributions for the six most important preequilibrium emission channels. The area under each of the curves represents the relative probability of complete fusion and preequilibrium emission in the indicated channels.

ergy, the average energy lost to preequilibrium emission was found to be 37 MeV. This corresponds to about a 20% reduction in excitation energy relative to the complete fusion value of 174 MeV. Rounding to the nearest  $Z$  and  $A$  (see Table II), on average preequilibrium emission reduces the charge of the compound system by one unit and the mass by three units corresponding to the compound nucleus  $^{115}\text{In}$ .

### C. Linear momentum transfer and fusionlike residues

As mentioned, both linear momentum transfer and tags on fusionlike residues have been used previously to estimate the compound nucleus excitation energy in heavy-ion collisions. In this section we calculate both the linear momentum transfer along the beam direction and the approximate velocity distribution of fusionlike residues using our preequilibrium particle multiplicities and excitation energies determined for  $^{18}\text{O}+^{100}\text{Mo}$  at 200 MeV.

As in our calculation of the mean energy lost to the compound system, we calculate the mean momentum removed from the compound system by taking the product of the average preequilibrium particle momentum with its multiplicity and then summing over particle types. Using  $A=118$  for the mass of a compound nucleus following complete fusion and  $A=115$  for the average mass for all fusionlike residues, we find a value of 92% of full linear momentum transfer, in good agreement with measured systematics [12,13]. We note that while the linear momentum transfer is reduced by only 8% relative to the complete fusion value, the excitation energy is reduced by the much larger factor of 20%.

Figure 10 shows an estimate of the residue velocity distribution, again using the determined multiplicities and energies for preequilibrium particles from  $^{18}\text{O}+^{100}\text{Mo}$  at 200 MeV. The calculation assumes that the preequilibrium particle emission probabilities are Poisson distributed about the average multiplicity and that there are no correlations between particles. The solid curves correspond to different preequilibrium particle emission channels and the area under each curve gives the relative probability for that channel. The shape of the distribution for complete fusion comes from

a Gaussian fit to a PACE calculation. The velocity distributions of the other channels are assumed to be the same except for a shift in average velocity and a scaling of the amplitude. In Fig. 10 one sees that the residue velocity distributions for both complete and incomplete fusion channels are broad and overlapping, making it difficult to use residue velocities to select events with a well-defined initial excitation energy. We note that any improvement in our simplifying assumptions of uncorrelated particle emission and constant velocity distributions will tend to make residues associated with complete fusion more difficult to separate from residues associated with preequilibrium events. In addition, these distributions are expected to become further broadened at higher bombarding energies.

### D. The GDR

Since the earliest observations of the GDR built on excited nuclear states, it was realized that the parameters which characterize the GDR in hot nuclei, the strength, width, and centroid energy are determined by the properties of the nuclei on which the resonance is built [36]. At relatively low bombarding energies, around 5 MeV/nucleon, it is a good approximation to say that all fusionlike events are, in fact, complete fusion events [37] so that the properties of the initial compound nucleus are well determined. This allows a rather straightforward analysis of measured GDR spectra in terms of a statistical model calculation. From bombarding energies of approximately 10 MeV/nucleon upward the range of masses and excitation energies corresponding to both complete and incomplete fusion should be taken into account when analyzing GDR  $\gamma$ -ray spectra from heavy-ion collisions.

It is well known that heavy-ion collisions in excess of 10 MeV/nucleon bombarding energy lead to a range of masses and excitation energies for the compound system. As a starting point, we represent the compound nuclei formed in  $^{18}\text{O}+^{100}\text{Mo}$  at 200 MeV bombarding energy by a compound nucleus with the average  $Z$ ,  $A$ , and excitation energy for all compound systems formed in the collisions. For the above reaction this was determined to be  $^{115}\text{In}$  with an initial excitation energy of 137 MeV. To estimate the effect of preequilibrium emission on the deduced GDR parameters, a  $\gamma$ -ray spectrum for  $^{115}\text{In}$  at this reduced excitation energy is generated using CASCADE, assuming reasonable GDR parameters [31,38,39]. This  $\gamma$ -ray spectrum is then fit using the complete fusion values for mass and excitation energy. Comparison of the fitted GDR parameters to the assumed parameters gives an estimate of the effect of preequilibrium emission on the deduced GDR parameters. The results of this calculation are summarized in Table III. Interestingly, both the deduced GDR width and strength are 15–20% lower if one fails to account for mass and energy lost to preequilibrium emission while the GDR centroid decreases by only 3%. These same reductions would be seen in a GDR analysis based on data normalized to  $\gamma$ -ray multiplicity per fusionlike event.

We note that if one had assumed complete fusion together with the CASCADE default fusion cross section, the deduced GDR strength would be nearly the same as a correct analysis which takes into account preequilibrium emission and the

TABLE III. Results of a CASCADE calculation to estimate the effects of preequilibrium energy loss on the GDR parameters. In the first row the  $Z$ ,  $A$ ,  $E^*$ , and  $\sigma_{\text{fus}}$  were determined experimentally for the reaction  $^{18}\text{O}+^{100}\text{Mo}$  at 200 MeV bombarding energy. Reasonable GDR parameters  $S$ ,  $\Gamma$ , and  $E_0$ , were chosen for  $^{115}\text{In}$ . The  $\gamma$ -ray spectrum for the decay of  $^{115}\text{In}$  is then fit assuming the decay of  $^{118}\text{Sn}$  at the full fusion excitation energy, and the deduced GDR fit parameters are shown.

Nucleus	$E^*$ (MeV)	$\sigma_{\text{fus}}$ (mb)	$S$	$\Gamma$ (MeV)	$E_0$ (MeV)
$^{115}\text{In}$	137	1700	1.00	9.00	15.00
$^{118}\text{Sn}$	174	1700	$0.81 \pm 0.01$	$7.7 \pm 0.1$	$14.53 \pm 0.04$

measured fusion cross section. This comes about, in this example, as an accidental cancellation between the increase in the fusionlike event cross section and the decrease in the average excitation energy due to incomplete fusion.

### V. SUMMARY

In this work we have measured preequilibrium light charged particles and fusionlike residue cross sections for  $^{18}\text{O}+^{100}\text{Mo}$  at 200 MeV bombarding energy. Preequilibrium particle multiplicities and energies, along with the measured fusion cross sections, permit a more realistic characterization of compound nuclei produced in these collisions. It was found that, on average, the compound nucleus excitation energy was reduced by approximately 20% and the mass by three nucleons relative to the complete fusion values. If neglected when performing a statistical model analysis, the mass and energy lost to preequilibrium emission at 200 MeV bombarding energy lead to a GDR width and strength that are 15–20% smaller than the values obtained taking into account preequilibrium emission.

Many GDR studies have been done involving projectile energies well in excess of 10 MeV/nucleon bombarding energy where incomplete fusion is certainly the dominant reaction channel leading to GDR  $\gamma$ -ray emission. Because preequilibrium emission must be increasingly large at higher bombarding energies, it is necessary to understand this effect well in order to interpret GDR spectra measured at high bombarding energy in terms of width and/or strength saturation. It is possible, in light of evidence that incomplete fusion is insensitive to the details of the target or projectile, that some general preequilibrium mass and excitation energy loss systematics can be developed for use in the study of heavy-ion collisions.

### ACKNOWLEDGMENTS

The authors gratefully acknowledge the input of Bob Vandenbosch and extend thanks for the use of the Fermi jet code. This work was supported in part by the U.S. Department of Energy.

- 
- [1] J. J. Gaardhøje, A. M. Bruce, J. D. Garrett, B. Herskind, M. Maurel, H. Nifenecker, J. A. Pinston, P. Perrin, C. Ristori, F. Schussler, A. Bracco, and M. Pignaneli, *Phys. Rev. Lett.* **59**, 1409 (1987).
  - [2] J. H. Le Faou, T. Suomijärvi, Y. Blumenfeld, P. Piattelli, C. Agodi, N. Alamanos, R. Alba, F. Auger, G. Bellia, Ph. Chomaz, R. Coniglione, A. Del Zoppo, P. Finocchiaro, N. Frascaria, J. J. Gaardhøje, J. P. Garron, A. Gillibert, M. Laméhi-Rachti, R. Liguori-Neto, C. Maiolino, E. Migneco, G. Russo, J. C. Roynette, D. Santonocito, P. Sapienza, J. A. Scarpaci, and A. Smerzi, *Phys. Rev. Lett.* **72**, 3321 (1994).
  - [3] T. Suomijärvi, Y. Blumenfeld, P. Piattelli, J. H. Le Faou, C. Agodi, N. Alamanos, R. Alba, F. Auger, G. Bellia, Ph. Chomaz, R. Coniglione, A. Del Zoppo, P. Finocchiaro, N. Frascaria, J. J. Gaardhøje, J. P. Garron, A. Gillibert, M. Laméhi-Rachti, R. Liguori-Neto, C. Maiolino, E. Migneco, G. Russo, J. C. Roynette, D. Santonocito, P. Sapienza, J. A. Scarpaci, and A. Smerzi, *Phys. Rev. C* **53**, 2258 (1996).
  - [4] A. Bracco, J. J. Gaardhøje, A. M. Bruce, J. D. Garrett, B. Herskind, M. Pignaneli, D. Barnéoud, H. Nifenecker, J. A. Pinston, C. Ristori, F. Schussler, J. Bacelar, and H. Hofmann, *Phys. Rev. Lett.* **62**, 2080 (1989).
  - [5] H. J. Hoffmann, J. C. Bacelar, M. N. Harakeh, T. D. Poelheken, and A. van der Woude, *Nucl. Phys.* **A571**, 300 (1994).
  - [6] G. Enders *et al.*, *Phys. Rev. Lett.* **69**, 249 (1992).
  - [7] W. E. Ormand, P. F. Bourignon, R. A. Broglia, T. Døssing, and B. Lauritzen, *Nucl. Phys.* **A519**, 61c (1993).
  - [8] Y. Alhassid, *Nucl. Phys.* **A553**, 137c (1993).
  - [9] P. F. Bourignon, A. Bracco, D. Brink, and R. A. Broglia, *Phys. Rev. Lett.* **67**, 3360 (1991).
  - [10] A. Smerzi, M. Di Toro, and D. M. Brink, *Phys. Lett. B* **320**, 16 (1994).
  - [11] Ph. Chomaz, *Nucl. Phys.* **A569**, 203c (1994).
  - [12] V. E. Viola, Jr., B. B. Back, K. L. Wolf, T. C. Awes, C. K. Gelbke, and H. Breuer, *Phys. Rev. C* **26**, 178 (1982).
  - [13] J. Jastrzebski, P. P. Singh, T. Mróz, H. J. Karwowski, S. E. Vigdor, and M. Fatyga, *Phys. Lett.* **136B**, 153 (1984).
  - [14] L. Westerberg, D. G. Sarantites, D. C. Hensley, R. A. Dayras, M. L. Halbert, and J. H. Barker, *Phys. Rev. C* **18**, 796 (1978).
  - [15] K. Geoffroy Young, D. G. Sarantites, J. R. Beene, M. L. Halbert, D. C. Hensley, R. A. Dayras, and J. H. Barker, *Phys. Rev. C* **23**, 479 (1981).
  - [16] T. C. Awes, S. Saini, G. Poggi, C. K. Gelbke, D. Cha, R. Legrain, and G. D. Westfall, *Phys. Rev. C* **25**, 2361 (1982).
  - [17] H. Tricoire, C. Gerschel, N. Perrin, H. Sergolle, L. Valentin, D. Bachelier, H. Doubre, and J. Gizon, *Z. Phys. A* **306**, 127 (1982).
  - [18] D. J. Parker, J. J. Hogan, and J. Asher, *Phys. Rev. C* **35**, 161 (1987).



- [19] D. Pierroutsakou, F. Auger, N. Alamanos, P. R. S. Gomes, J. L. Sida, A. Gillibert, N. Frascaria, I. Lhenry, J. C. Roynette, and T. Suomijärvi, *Nucl. Phys.* **A600**, 131 (1996).
- [20] M. P. Kelly, Ph.D. research, University of Washington.
- [21] J. F. Liang, J. D. Bierman, M. P. Kelly, A. A. Sonzogni, R. Vandenbosch, and J. P. S. van Schagen (unpublished).
- [22] J. Randrup and R. Vandenbosch, *Nucl. Phys.* **A474**, 219 (1987).
- [23] S. J. Luke, R. Vandenbosch, and J. Randrup, *Phys. Rev. C* **48**, 857 (1993).
- [24] D. Prindle, R. Vandenbosch, S. Kailas, A. Charlop, and C. Hyde-Wright, *Phys. Rev. C* **48**, 291 (1993).
- [25] W. Reisdorf, *Z. Phys. A* **300**, (1981).
- [26] C. Gershel, A. Gillibert, N. Perrin, and H. Tricoire, *Z. Phys. A* **322**, 433 (1985).
- [27] D. J. Hinde *et al.*, *Nucl. Phys.* **A385**, 109 (1982).
- [28] S. Cohen, F. Plasil, and W. J. Swiatecki, *Ann. Phys. (N.Y.)* **82**, 557 (1974).
- [29] R. Bass, *Nucl. Phys.* **A231**, 45 (1974).
- [30] A. J. Sierk, *Phys. Rev. C* **33**, 2039 (1986).
- [31] J. J. Gaardhøje, *Annu. Rev. Nucl. Part. Sci.* **42**, 483 (1992).
- [32] J. R. Beene, M. L. Halbert, D. C. Hensley, R. A. Dayras, K. Geoffroy Young, D. G. Sarantites, and J. H. Barker, *Phys. Rev. C* **23**, 2463 (1981).
- [33] D. L. Hillis, J. D. Garret, O. Christensen, B. Fernandez, B. B. Back, and F. Folkmann, *Nucl. Phys.* **A325**, 216 (1979).
- [34] K. A. Geoffroy Young, D. G. Sarantites, M. L. Halbert, D. C. Hensley, R. A. Dayras, and J. H. Barker, *Phys. Rev. Lett.* **43**, 1030 (1979).
- [35] A. Gavron, J. R. Beene, R. L. Ferguson, F. E. Obenshain, F. Plasil, G. R. Young, G. A. Petitt, K. Geoffroy Young, M. Jääskeläinen, D. G. Sarantites, and C. F. Maguire, *Phys. Rev. C* **24**, 2048 (1981).
- [36] J. O. Newton, B. Herskind, R. M. Diamond, E. L. Dines, J. E. Draper, K. H. Lindenberg, C. Schüch, S. Shih, and F. S. Stephens, *Phys. Rev. Lett.* **46**, 1383 (1981).
- [37] I. Tserruya, V. Steiner, Z. Fraenkel, P. Jacobs, D. G. Kovar, W. Henning, M. F. Vineyard, and B. G. Glagola, *Phys. Rev. Lett.* **60**, 14 (1988).
- [38] B. L. Berman and S. C. Fultz, *Rev. Mod. Phys.* **47**, 713 (1975).
- [39] K. A. Snover, *Annu. Rev. Nucl. Part. Sci.* **36**, 545 (1986).